Z. Physik 268, 57–64 (1974)

Spectra of Neutrons from μ Capture in Thallium, Lead and Bismuth*

W. U. Schröder

Institut für Kernphysik der Technischen Hochschule Darmstadt, Germany

U. Jahnke, K. H. Lindenberger and G. Röschert

Hahn-Meitner-Institut für Kernforschung Berlin GmbH, Germany

R. Engfer and H. K. Walter

Laboratorium für Hochenergiephysik der ETH-Zürich, Villigen, Switzerland

Received January 11, 1974

Abstract. The energy distributions of neutrons from μ capture in Tl, Pb, and Bi were measured applying a time-of-flight technique, using de-excitation γ-rays from final nuclei as a time reference. The spectra exhibit an evaporation part, which is described by nuclear temperatures varying from $\theta = 1.06$ MeV for Bi to $\theta = 1.22$ MeV for Pb, and an exponentially decreasing high-energy distribution with a relative intensity of $\sim 10\%$, which is interpreted, on the basis of a simple model, as being due to direct and pre-compound processes.

1. Introduction

The weak interaction between a negative muon and a nucleus $A(Z, N)$ is well known [1]. Therefore, the μ-capture process

$$\mu^- + A(Z, N) \rightarrow \nu + A^*(Z-1, N+1) \quad (1)$$

provides a tool to study nuclear properties. By this reaction a high excitation energy, up to the muon rest energy $m_\mu c^2 = 105$ MeV, may be stored in the nucleus.

The μ-capture reaction can be studied by the observation of the induced γ and neutron radiation. Especially, the spectrum of neutrons emitted after μ capture may supply information on the reaction mechanism. The decay of highly-excited compound states formed in the capture will give rise to an evaporation-type spectrum. However, neutrons emitted directly or from early stages of the energy-dissipation process within the nucleus will show a broad distribution reaching up to high energies, which provides a test of the high-momentum components of the nuclear wavefunction. The contribution of the direct-neutron emission was considered by several authors applying a Fermi gas model [2, 3], Brueckner's model [4] or, for light nuclei, a single-particle model [2, 5–8]. Some of the calculations [2, 3, 5, 7, 8] accounted for the final-state interaction of the emerging neutron by an optical potential. The experimental spectra [9] of neutrons from light nuclei for energies higher than 20 MeV are well described by the theory. However, there seem to be discrepancies at lower energies [6, 8]. The μ capture through resonances would result in a line structure of the neutron spectrum [10, 11], which is determined by the selection rules for the decay of the resonant states. Experiments [12, 13] yielded evidence for such structure in the total neutron spectrum of some light nuclei.

Little is known experimentally, or theoretically, about the neutron spectra from heavy nuclei. In the case of lead, the Fermi-gas calculations [2, 3], lead to a

* Part of this work is the subject of a Ph. D. Thesis D 17, Technische Hochschule Darmstadt, by W. U. Schröder.

complete disagreement with the experimental [9, 12, 14–16] high-energy neutron spectrum.

This paper reports on measurements of the energy spectra of neutrons from μ capture in thallium, lead and bismuth, in coincidence with de-excitation γ-rays using a time-of-flight technique. Parts of the results have already been reported earlier [16]. The experimental method, as well as details of the measurements and the evaluation of data, are described in Section 2. The results are presented in Section 3. Section 4 gives an interpretation of the high-energy spectrum by means of an extension of Singer's model [4]. Section 5 includes a further discussion of the results.

2. The Experiment

In order to avoid the unfolding procedure associated with proton-recoil techniques of previous experiments, the neutron energy was measured with a time-of-flight spectrometer. De-excitation γ-rays from final nuclei provided signals to start the time-of-flight measurement, because the neutron emission and the subsequent γ transitions occur simultaneously within the spectrometer resolution. An attempt was also made to distinguish between different γ transitions in order to separate neutron transitions to different final isotopes and excited states. As a compromise between efficiency, energy and time resolution, a NaI scintillator was chosen for the start detector.

The experiments were performed at the backward muon beam at the CERN Synchro-cyclotron. About 5×10^4 muons per second were incident on the counter array shown in Fig. 1, and of these 20% were stopped in the target. The muon telescope, consisting of four plastic counters (1 to 4 in Fig. 1), was used to detect a muon stop in the target by the coincidence requirement $123\bar{4}$. A block of ~ 7 cm graphite between counters 2 and 3 moderated the muons. Counter 4, a five-sided scintillator box containing the target, vetoed muons not stopped in the target. The target was inclined by 45° with respect to the beam direction in order to obtain a high stopping rate and a low absorption of γ-rays and neutrons in the direction of the detectors. The NaI detector was located at an optimum distance of ~ 8 cm from the target and protected from the beam by lead shielding. The neutron detector was placed perpendicular to the target. A 1 mm thick plastic shield detector in front of the neutron counter prevented charged particles from being recorded.

The NaI detector was a crystal of 2 in. × 2 in. diameter mounted on a 56 AVP photomultiplier. The energy resolution at 1 MeV was 9% and its time resolution

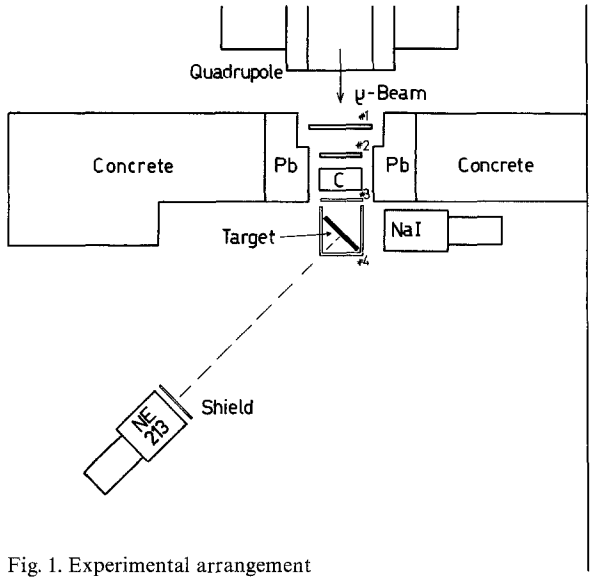

Fig. 1. Experimental arrangement

1.5 nsec. The neutron detector consisted of a liquid scintillator NE 213 of 2 in. × 5 in. diameter on an XP 1040 multiplier. The pulse-shape discrimination circuit provided a γ-rejection factor of ~ 100. The time resolution of the neutron detector was typically 1.5 nsec for γ-rays between 0.1 and 2.5 MeV. The total time resolution of the spectrometer amounted to $\lesssim 3.5$ nsec during the experiments. For a flight distance of 1 m, this corresponds to a neutron-energy resolution of 10% at 1 MeV and 25% at 5 MeV.

The electronic set-up shown in Fig. 2 served to measure simultaneously the neutron time of flight and the energy of the γ-ray. Fast triggers provided timing signals from the plastic counters; constant-fraction timing discriminators were used for the NaI and the neutron detectors. The coincidence signal $123\bar{4}$, indicating a muon stop in the target, was used to generate a gate pulse defining the time interval during which a γ event could be taken to originate from a μ-capture process. This gate was delayed by 20 nsec with respect to the prompt muonic X-rays. The length of the gate (250 nsec) was chosen to give an optimum value of the true-event to background ratio. The gate was inhibited, if the signal from the NaI counter was in prompt coincidence with a signal from the 10 in. × 10 in. telescope counter 1 covering the whole solid angle accessible by the muon beam. By this means the measurement was protected from the prompt muonic X-rays produced by a second muon impinging on the counter array after a muon stop. Another protection circuit rejected also delayed events generated by a second muon, detected during the time measurement. Events in the γ detector not vetoed by these require-

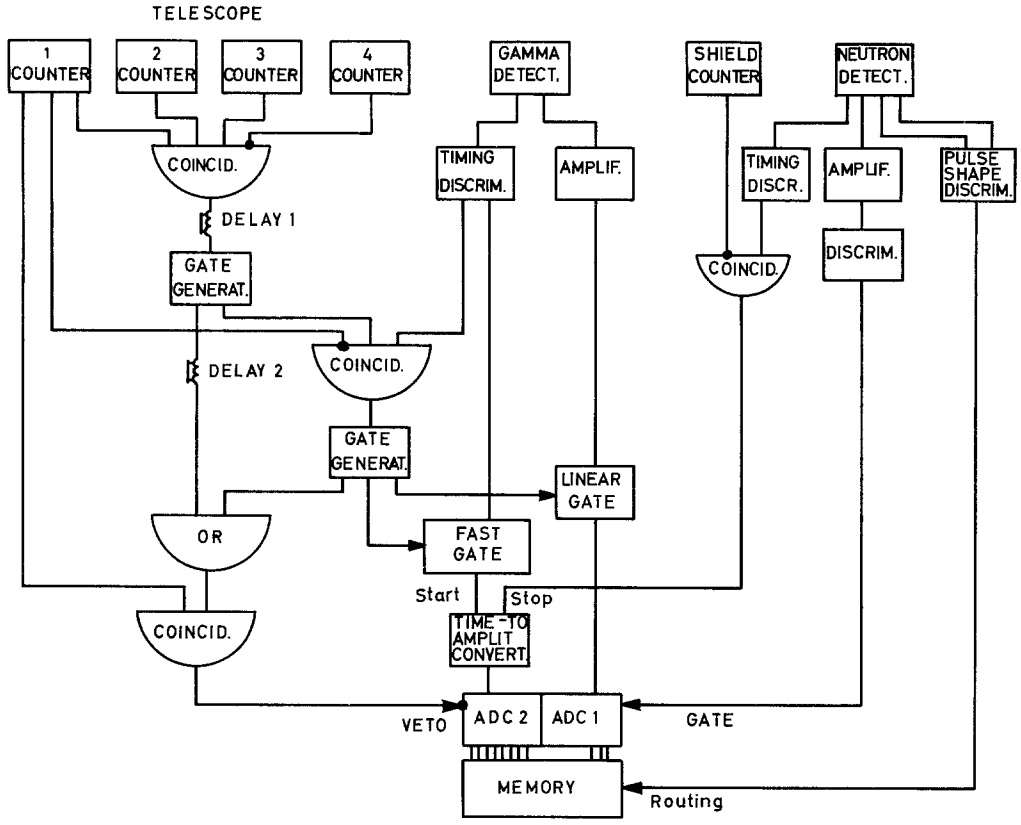

Fig. 2. Simplified block diagram of the electronics. See explanation in text

ments started a time-to-amplitude converter (TAC). The time measurement was stopped by a timing signal from the neutron detector, which was vetoed by signals from the shield counter.

The time-of-flight spectra from the TAC were sorted into 256 channels by ADC 2, driven in two-dimensional mode with ADC 1 sorting the spectrum of delayed γ-rays into 8 channels. The protection circuit and the neutron-detection threshold discriminator operated on the input gates of the ADC's. The signals from the γ-neutron identification circuit were used for routing to the two halves of a 4096 channel memory.

3. Measurements and Results

Measurements were performed during 70 to 100 h per target at a flight distance of 1 m. Consistency checks were made at 0.5 m flight distance. The targets were of natural isotopic abundance and in the form of rectangular metal plates of 2 to 4 g/cm^2 effective thickness. The total rate of γ-neutron coincidences amounted to 10 to 20 counts per minute.

The spectra of delayed γ-rays taken with the NaI detector were interpreted with the aid of high-resolution measurements using Ge(Li) detectors [17–19]. Fig. 3 presents the NaI spectrum of delayed γ-rays obtained from the bismuth target. The spectrum is easily interpreted, since bismuth is a pure isotope element, and the level schemes of the lead isotopes formed in the capture process are well known. The main γ lines correspond to the 0.583 MeV and the 2.614 MeV transitions belonging to the $5^- \rightarrow 3^- \rightarrow 0^+$ γ cascade in ^{208}Pb. In Fig. 3, the 2.614 MeV line is clearly exhibited, together with its escape peaks and its Compton distribution. The 0.583 MeV ^{208}Pb line is not resolved from the 0.569 MeV ^{207}Pb line. Their relative intensities are 3:2 in the single spectrum. However, the relative contributions of different γ transitions are enhanced, in the coincidence spectrum, according to the number of preceding neutron transitions. Other transitions in ^{206}Pb and ^{207}Pb are not isolated from ^{208}Pb transitions, since the high Compton background of the 2.614 MeV line is always superimposed. At the bottom of Fig. 3, the 8 γ-energy channels are indicated, corresponding to which the time-of-flight spectra were accumulated.

In the cases of thallium and lead, the identification of μ-capture transitions is even more difficult than

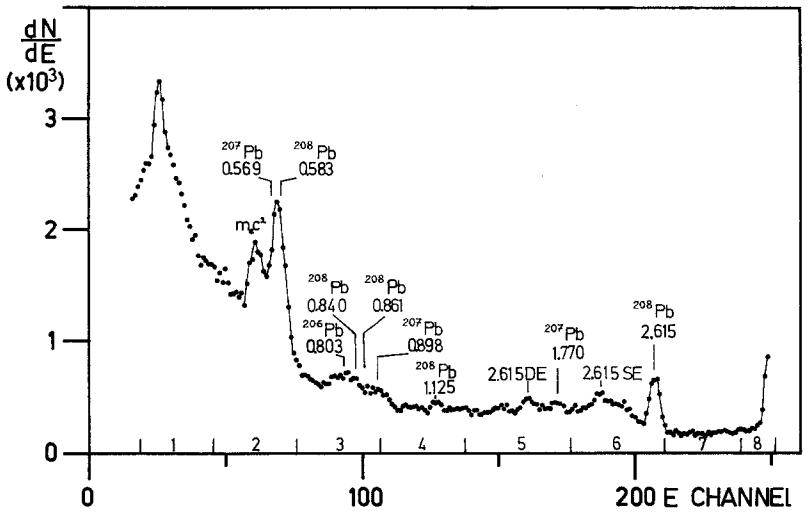

Fig. 3. NaI spectrum of delayed γ-rays from μ capture in Bi. Energies are given in MeV. At the bottom of the spectrum the 8 energy channels are indicated, corresponding to which the time-of-flight spectra were accumulated. The rise at the high-energy end is due to the saturation of the amplifier

for bismuth, since those elements are not monoisotopic and the energy spectra of the residual nuclei are not sufficiently well known. The 0.439 MeV ^{202}Hg line, for example, results from both the reactions ^{203}Tl$(\mu, \nu\, n)^{202}$Hg and ^{205}Tl$(\mu, \nu\, 3n)^{202}$Hg. Assuming a ratio of 4.6 for the probabilities of the processes $(\mu, \nu\, n)$ to $(\mu, \nu\, 3n)$, as found experimentally in bismuth [18], and taking into account the isotopic abundance, about 66% of the intensity of the 0.439 MeV line is due to the reaction ^{203}Tl$(\mu, \nu\, n)^{202}$Hg. However, in the γ spectrum coincident with neutrons, the ^{205}Tl$(\mu, \nu\, 3n)^{202}$Hg reaction is responsible for 60% of this intensity. Similar arguments hold also for most of the other γ transitions after μ capture in thallium and lead.

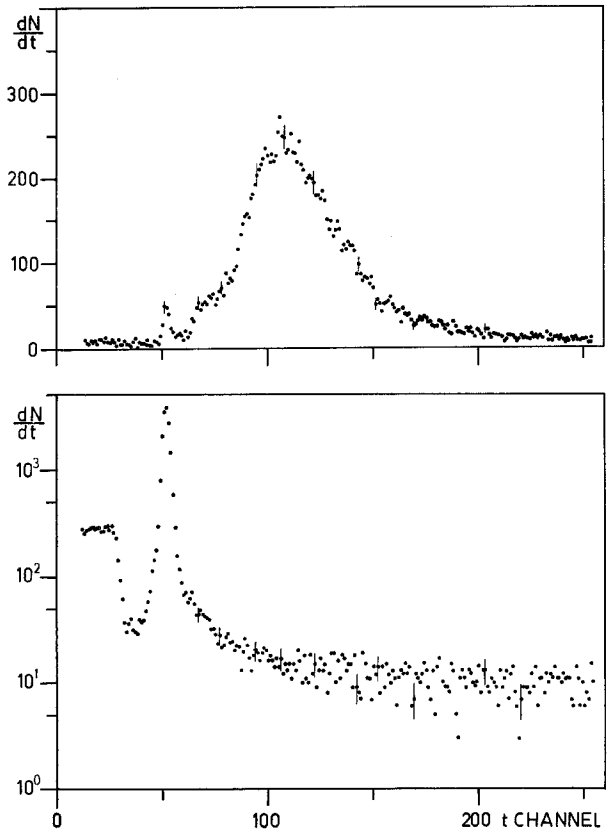

In Fig. 4 the time-of-flight spectra obtained in a 50 h thallium run are shown. The peak in the γ spectrum at channel 52 originates from coincident detection of delayed cascade γ-rays in both detectors. It is also present in the neutron spectrum but suppressed by the pulse-shape discrimination circuit. In the neutron time-of-flight spectrum, a continuous distribution of neutrons can be seen on the right of the small γ peak.

The spectra were corrected for the energy dependence of the timing, which could be deduced from the positions of the γ peak for a given γ-energy range. A constant background was fitted to the late-time end of the neutron spectrum and then subtracted. For subtracting the γ peak, only its intensity was fitted in the neutron spectrum. Line shape and position were determined from the γ spectrum. The uncertainty in determining the background was accounted for in the numerical results. The time-of-flight spectrum was converted to energy scale referring to the γ-peak position and corrected for the neutron-detection efficiency. The resulting neutron-energy spectra are displayed in Fig. 5.

Fig. 4. Time-of-flight spectrum of neutrons (top) and γ-rays (bottom, logarithmic scale) from μ capture in Tl measured at 1 m flight distance. The time calibration is 0.9 nsec/channel. The peak at channel 52 in both spectra is due to delayed γ-rays coincident in neutron and γ detectors

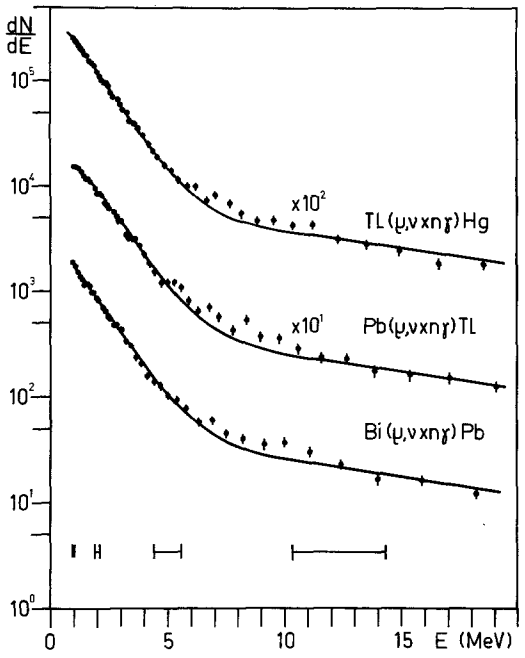

Fig. 5. Spectra of neutrons from μ capture in Tl, Pb and Bi. The ordinate gives the number of counts for the Bi spectrum; the other spectra have been displaced for better display. The horizontal bars indicate the energy resolution. The curves represent calculations explained in Section 4

In the energy range from 1 to 4 MeV, the neutron spectra can be fitted to an evaporative form [20]

$$\frac{dN(E)}{dE} \sim E^{5/11}\, e^{-E/\theta}, \tag{2}$$

where θ is the effective nuclear temperature. The nuclear temperature parameters obtained are collected in Table 1. For comparison with other investigations, an exponential, $dN'/dE \sim \exp(-E/E_d)$, was fitted to the spectra for $E > 4.5$ MeV. We find $E_d = (9 \pm 1)$ MeV for thallium and lead, and $E_d = (8 \pm 1)$ MeV for bismuth. The fractional intensity F of the high-energy distribution, integrated from 4.5 to 20 MeV and normalized to the total spectrum, is also included in Table 1. There was no significant line structure observed in the neutron spectra of thallium, lead and bismuth.

Table 1. Nuclear temperature parameter θ and fractional intensity F ($4.5 < E < 20$ MeV) of the high-energy neutron distribution

Target element	θ [MeV]	F
Tl	1.09 ± 0.04	0.096 ± 0.008
Pb	1.22 ± 0.06	0.102 ± 0.010
Bi	1.06 ± 0.05	0.097 ± 0.010

For each target, the temperature parameter θ and the fractional intensity F were also determined from the neutron spectra corresponding to the 8 different γ-energy channels. The nuclear temperature was found to be constant with energy, within the experimental errors of 5 to 10%. The high-energy contribution F could be determined for the different γ-energy channels only with an accuracy of $\sim 20\%$. Within these errors, F remained constant with varying γ energy.

4. Calculations

The failure of the Fermi gas calculations [2, 3] to explain the high-energy part of the neutron spectrum, and the lack of detailed calculations on heavy nuclei may justify the application of Singer's simple model [4] to this problem. This model is based on Brueckner's theory on nuclear matter and has successfully predicted μ-capture neutron multiplicities for a range of medium-weight and heavy nuclei [18, 21, 22]. In the model, the capturing nucleus is characterized by a Gaussian nucleon momentum distribution; any details of the weak interaction Hamiltonian are neglected, whereas the Pauli principle is taken into account. Singer's model was extended to predict also the spectra of neutrons emitted in direct and other pre-compound processes. Some results of the work of Lubkin [2] and Hagge [3] were incorporated in the calculations.

Singer wrote the total capture rate as an integral over the excitation function of the μ-capture reaction. This may be transformed into an integral over the energy distribution of the neutrons created within the nucleus, yielding

$$\frac{d\tilde{N}(E)}{dE} \sim e^{-\beta(E-E_0)}(1-e^{-\beta E}) \cdot \left\{\left(\varepsilon+\frac{1}{\beta}\right) e^{-\beta E} - \left(E_0+\frac{1}{\beta}\right) e^{-\beta E_0}\right\}, \tag{3}$$

where $\beta = 2m^*/\alpha^2$, m^* being the effective nucleon mass, α the $1/e$ width of the nucleon momentum distribution, and

$$\varepsilon = m^* c^2 + (2m^* c^2 E)^{\frac{1}{2}} - \{[m^* c^2 + (2m^* c^2 E)^{\frac{1}{2}}]^2 - 2m^* c^2 E_0\}^{\frac{1}{2}} \tag{4}$$

is the minimum neutrino energy for a given neutron energy. E denotes the neutron kinetic energy within the nucleus, and E_0 is the Q-value of the reaction.

The escape probability $T_a(E, r)$ of a neutron created with an energy E at a point r within the nucleus was calculated within the semi-classical optical model [2, 3]. Here, individual neutrons are followed along their tracks within the nucleus, describing the absorp-

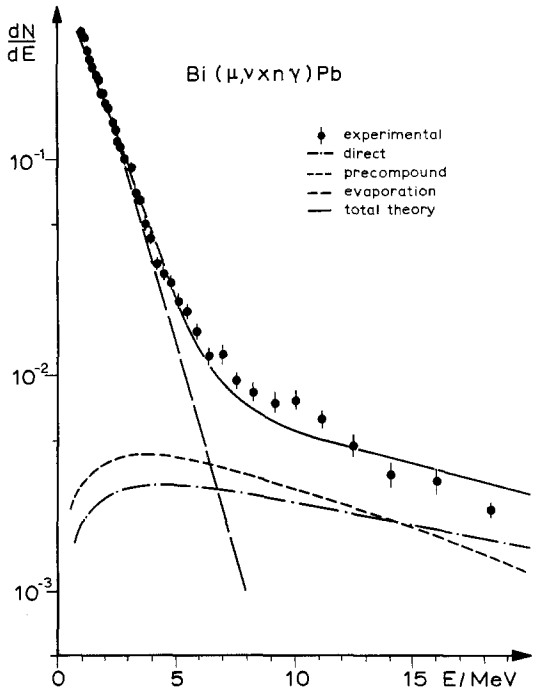

Fig. 6. Experimental and theoretical neutron spectrum of Bi. The ordinate scale is given in units per capture. The experimental spectrum has been normalized to fit the theoretical one. For further explanation see Section 4

tion in the nucleus and the reflection at the nuclear surface by a mean free path and a refractive index, respectively, derived from the nuclear optical potential. The distribution over the nuclear volume of the primary neutrons was assumed to be proportional to the muonic 1s density distribution as given by Pustovalov [23]. A square-well optical potential

$$V(E)=(-47.0\ \mathrm{MeV}+0.25\,E)-i(3.5\ \mathrm{MeV}+0.43\,E) \quad (5)$$

with a radius of $R=1.3\,A^{\frac{1}{3}}$ fm was used. E is the neutron kinetic energy outside the nucleus. This potential is an approximation of the one quoted by Fu and Perey [24] and reproduces also the mean free path obtained by Kikuchi and Kawai [25].

With a width of the nucleon momentum distribution $\alpha^2/2m=20$ MeV and an effective nucleon mass $m^*=0.68\,m$, where m is the free nucleon mass, and the potential of Eq. (6), the neutron multiplicity distribution according to Singer's model and the spectrum of directly emitted primary neutrons were calculated for ^{209}Bi. A good agreement between theoretical and experimental [18] multiplicities was achieved. The theoretical direct neutron spectrum depicted in Fig. 6 extends to much higher energies than predicted by the Fermi gas calculations [2, 3]. However, its contribution in the energy range from 5 to 20 MeV to the total spectrum amounts only to $\sim 5\%$, compared to the experimental intensity F of $\sim 10\%$ (cf. Table 1). The agreement cannot be improved by changing the model parameters within reasonable limits, if also a consistent description of the experimental neutron-multiplicity distribution is required.

Because of this discrepancy, the successive scattering of the absorbed nucleons on the other bound nucleons was accounted for, up to second order. Requiring energy conservation and the Pauli principle for the scattered nucleons, the following energy spectrum of secondary neutrons, i.e. of the "pre-compound" neutrons, was obtained:

$$\frac{dN_p(E)}{dE}=\int d^3r\ T_d(E,r)\,(1-e^{-\beta E})\int_E^\infty dE'\,\{N_1(E')\,Q(E',r)\,[1-e^{-\beta E}-\tfrac{1}{2}(e^{-\beta(E'-E)}-e^{-\beta(E'+E)})]+e^{-\beta(E'+E)}(1-e^{-\beta E'})\int_{E'}^{E'+E} dE''\,N_2(E'')\,Q(E'',r)\}. \quad (6)$$

The two terms in curly brackets denote the contributions from the two scattering partners. In order to avoid double counting, the spectrum of absorbed nucleons was properly normalized to both contributions, to give $N_1(E')$ and $N_2(E'')$, respectively. $Q(E,r)$ stands for the radial dependence of the absorption rate of primary neutrons of a given energy E, i.e. the source-density distribution of the pre-compound neutrons. In a further simplification, the emission of protons was neglected, since it is strongly suppressed by the Coulomb barrier, in heavy nuclei. Two successive scatterings were considered, using Eq. (6) iteratively.

The resulting pre-compound neutron spectrum of ^{209}Bi, using the parameter set quoted above, is also shown in Fig. 6. The shapes of the direct and pre-compound neutron spectra are quite similar. However, the pre-compound neutron spectrum decays faster than the direct-neutron spectrum, with increasing energy. The sum intensity of both contributions in the range from 5 to 20 MeV amounts to $\sim 7\%$ of the total spectrum, which is close to the experimental value. The energy integrated intensity of the sum spectrum yields ~ 0.14 per capture. Assuming that with a probability of ~ 0.86 a compound nucleus is formed in the capture process, resulting in an evaporative neutron spectrum [cf. Eq. (2)], the total theoretical spectrum indicated in Fig. 6 is obtained. Here, only the temperature parameter θ was taken from the experiment. The agreement with the experimental spectrum is satisfactory. The same is true for the lead and thallium neutron spectra depicted in Fig. 5, calcu-

lated using the same model parameters, and the experimental nuclear temperature. A good agreement was also obtained with the experimental results of Krieger [14], who has measured absolutely the spectrum of neutrons from μ capture in lead, in the energy range from ~ 10 to ~ 50 MeV.

It should be noticed that there are over-simplifications and ambiguities in the model. This applies for the μ-capture Hamiltonian and the semi-classical optical model overestimating the reflection of neutrons at the nuclear boundary. Also, the results depend strongly on the optical model parameters. More details are given in a separate report [26].

5. Discussion of the Results

Prior to this experiment no γ-neutron coincidence experiments on the spectra of neutrons from μ capture have been published. However, Hagge [3] and Evseyev *et al.* [12] have performed measurements on the total neutron spectrum from lead, to which the present results may be compared. The spectra obtained by those authors are quite similar to the one presented here. Hagge finds a nuclear temperature of $\theta = (1.35 \pm 0.17)$ MeV; Evseyev *et al.* quote $\theta = (1.15 \pm 0.20)$ MeV. The present value agrees with both these results within the errors (cf. Table 1). Our high-energy decay constant E_d is also in agreement with the data of Evseyev *et al.* and consistent with the spectrum of Krieger [14]. However, the spectrum measured by Hagge seems to drop by a factor of ~ 2 faster with increasing energy than the present one.

Within the experimental accuracy, there is no significant deviation of the lead neutron spectrum of Evseev *et al.* from the one reported on here, although those authors measured the spectrum, including neutron transitions to ground states, without any coincidence requirements. In this work, the coincidence efficiency depends on the number of γ-rays correlated with a specific neutron transition and their energies; neutron-ground-state transitions are not detected. Within the statistical accuracy and the experimental resolution no correlation between the high-energy fraction F and the γ-ray energy was found.

The high-energy part of the neutron spectrum is interpreted by the calculations briefly described in the preceding section to be due to the direct and pre-compound emission processes. Although the capture is treated in an over-simplified and incomplete manner, the agreement with the experimental spectra is good (cf. Figs. 5, 6). The discrepancy in the range from 5 to 10 MeV may be due to the restricted number of pre-compound scattering processes considered.

In spite of the shortcomings of the model, one may infer from the calculations and the experimental spectra, that direct or pre-compound neutron emission occurs with a probability of $\gtrsim 0.15$ after μ capture in heavy elements. Both processes are of similar importance for neutron energies lower than ~ 20 MeV. Although at higher energies direct processes are dominant, pre-compound emission is still not negligible.

It is interesting to compare μ capture in heavy nuclei with photo-absorption reactions, since there are marked similarities at the light nuclei. In the lead region, the spectra of neutrons from (γ, n) reactions were found experimentally [27, 28] to consist mainly of an evaporation part, the corresponding temperature being $\theta = 1.0$ to 1.5 MeV. In addition, a high-energy tail with a relative intensity of 15 to 20% was observed, which was attributed to the direct emission process. So far, μ capture yields similar results to photo-absorption. However, the (γ, n)-neutron spectra from lead and bismuth [28, 29] exhibited fine structure, which could be related [29] to peaks in the (γ, n) cross-section. In the μ-capture neutron spectra, we do not observe a similarly pronounced structure. This could be due to the fact, that μ capture in heavy nuclei is less selective than photo-absorption.

This work is part of the research programme of the Berlin-Darmstadt-Fribourg-Zürich Collaboration at CERN. The authors would like to express their thanks to Dr. H. Backe, Prof. E. Kankeleit, Dr. C. Petitjean and Dr. H. Schneuwly for their help during the experiments. The kind hospitality of the CERN Nuclear Physics Division is gratefully acknowledged.

This work was supported by the Bundesministerium für Bildung und Wissenschaft.

References

1. Balashov, V.V., Eramzhyan, R.A.: Atom. En. Rev. **5** (3), 3 (1967)
2. Lubkin, E.: Ann. Phys. (USA) **11**, 414 (1960)
3. Hagge, D.E.: Thesis, UCRL-10516. Univ. of California 1963
4. Singer, P.: Nuovo Cimento **23**, 669 (1962)
5. Dolinsky, E.I., Blokhintzev, L.D.: Nuclear Phys. **10**, 527 (1959)
6. Bogan, A., Jr.: Nuclear Phys. B **12**, 89 (1969)
7. Madurga, G.: GIFT. 3/72. Univ. de Barcelona 1972
8. Boussy, A., Ngo, H., Vinh Mau, N.: IPNO/TH 73-2. Orsay 1973
9. Sundelin, R.M., Edelstein, R.M., Suzuki, A., Takahashi, K.: Phys. Rev. Letters **20**, 1198 (1968)
10. Balashov, V.V., Beliaev, V.B., Eramjian, R.A., Kabachnik, N.M.: Phys. Letters **9**, 168 (1964)
11. Überall, H.: Phys. Rev. **139** B, 1239 (1965)
    Hill, L.L., Überall, H.: Nuclear Phys. A **190**, 341 (1972)
12. Woitkowska, J., Evseyev, V.S., Kozlowski, T., Mamedov, R.N., Roganov, V.S.: Sov. J. Nuclear Phys. **14**, 349 (1972)
13. Plett, M.E., Sobottka, S.E.: Phys. Rev. **3**C, 1003 (1971)
14. Krieger, M.H.: Thesis, NEVIS-172. Columbia Univ. 1969
15. Schröder, W.U.: Thesis, TH Darmstadt 1971
16. Jahnke, U., Lindenberger, K.H., Röschert, G., Schröder, W.U., Backe, H., Engfer, R., Kankeleit, E., Schneuwly, H., Vuilleumier, J.L., Walter, H.K.: Helv. Phys. Acta **45**, 49 (1972)

17. Backe, H., Engfer, R., Jahnke, U., Kankeleit, E., Pearce, R. M., Petitjean, C., Schellenberg, L., Schneuwly, H., Schröder, W. U., Walter, H. K., Zehnder, A.: Nuclear Phys. A **189**, 472 (1972)
18. Zehnder, A.: Diplomarbeit. ETH Zürich 1970
19. Schröder, W. U., Vuilleumier, J. L.: In preparation
20. Le Couteur, K. J.: in Nuclear reactions, Eds. P. M. Endt and M. Demeur. Amsterdam: North Holland 1959
21. Petitjean, C., Backe, H., Engfer, R., Jahnke, U., Lindenberger, K. H., Schneuwly, H., Schröder, W. U., Walter, H. K.: Nuclear Phys. A **178**, 193 (1971)
22. Backenstoss, G., Charalambus, S., Daniel, H., Hamilton, W. D., Lynen, U., Von der Malsburg, Ch., Poelz, G., Povel, H. P.: Nuclear Phys. A **162**, 541 (1971)
23. Pustovalov, G. E.: Soviet Phys. JETP **9**, 1288 (1959)
24. Fu, C. Y., Perey, F. G.: ORNL-4765, 1972
25. Kikuchi, K., Kawai, M.: Nuclear matter and nuclear reactions. Amsterdam: North Holland 1968
26. Schröder, W. U.: IKDA 73-17. TH Darmstadt 1973
27. Zatsepina, G. N., Igonin, V. V., Lazareva, L. E., Lepestkin, A. I.: Soviet Phys. JETP **17**, 1200 (1963)
28. Glazunow, Yu. Ya., Savin, M. V., Safina, I. N., Fomushkin, E. F., Khokhlov, Yu. A.: Soviet Phys. JETP **19**, 1284 (1964)
29. McNeill, K. G., Jury, J. W., Hewitt, J. S.: Canad. J. Phys. **48**, 950 (1970)

Dr. W. U. Schröder
Institut für Kernphysik, Technische Hochschule Darmstadt
D-6100 Darmstadt
Schloßgartenstraße 9
Federal Republic of Germany

Prof. K. H. Lindenberger
Dr. U. Jahnke
Dr. G. Röschert
Hahn-Meitner-Institut für Kernforschung Berlin GmbH
D-1000 Berlin 39
Glienicker Straße 100

Dr. R. Engfer
Dr. H. K. Walter
Laboratorium für Hochenergiephysik der ETH-Zürich
Villigen/Switzerland